Scientific African 26 (2024) e02455

Contents lists available at ScienceDirect

Scientific African

journal homepage: www.elsevier.com/locate/sciaf

"Hydroethanol extract and triterpenoids of *Senegalia ataxacantha* show antiplasmodial activity and the compounds are predicted to inhibit parasite lactate dehydrogenase (pfLDH) as indicated by molecular docking studies"

Kennedy Ameyaw Baah [a,b], Akwasi Acheampong [a,*], Isaac Kingsley Amponsah [c], Silas Adjei [c], Yakubu Jibira [d], Reinhard Isaac Nketia [e], Linda Mensah Sarpong [a], Emmanuel Quaye Kontoh [c]

[a] *Department of Chemistry, Faculty of Physical and Computational Sciences, College of Science, Kwame Nkrumah University of Science and Technology, Kumasi, Ghana*
[b] *Department of Science Education, Wesley College of Education, Kumasi, Ghana*
[c] *Department of Herbal Medicine, Faculty of Pharmacy and Pharmaceutical Sciences, College of Health Science, Kwame Nkrumah University of Science and Technology, Kumasi, Ghana*
[d] *Department of Pharmacology and Toxicology, School of Pharmacy and Pharmaceutical Sciences, University for Development Studies, Tamale, Ghana*
[e] *Department of Pharmacognosy, Faculty of Pharmacy and Pharmaceutical Sciences, College of Health Science, Kwame Nkrumah University of Science and Technology, Kumasi, Ghana*

ARTICLE INFO

Editor: DR B Gyampoh

Keywords:
Antipyretic
In silico
Structural elucidation
Chromatographic fractionation
Antimalaria
Pharmacokinetic profile

ABSTRACT

Malaria claims over 600,000 deaths annually with a disproportionately high burden in the WHO African Region. The development of parasite resistance has warranted the search for novel anti-plasmodial drug candidates. This research aimed at validating the efficacy of *Senegalia ataxacantha* and tracking down its bioactive constituents. *In vivo* antiplasmodial activity of the extract was assessed using suppressive and curative protocols. Yeast-induced pyrexia was employed to evaluate the antipyretic activity of the extract. *In vitro* anti-plasmodial activity of isolated compounds was done using SYBR green I fluorescence assay on chloroquine sensitive (3D7) and resistant (Dd2) strains of *P falciparum. In silico* pharmacokinetic and interactions with parasites lactate dehydrogenase predictions of isolated compounds was conducted through molecular docking studies. Ethanol (70 %) extract of the plant showed *in vitro* and *in vivo* anti-plasmodial effect. The extract demonstrated significant ($p < 0.05$) dose-dependent suppression of 63.39 % and 63.32 % respectively at the highest dose (300 mg kg^{-1}). Artesunate (4 mg kg^{-1}/day) had considerably better curative potential (85.25%). The compounds showed *in vitro* anti-plasmodial activity in the order lupeol> friedelin/ friedelinol mixture>friedelin>β-sitosterol based on IC_{50} measurement. Friedelinol and lupeol exhibited higher binding affinities with pfLDH compared to Chloroquine. The extract and acetaminophen (positve control) showed significant ($p < 0.05$) reduction in rectal temperature compared to the control group. *In silico* studies of the compounds revealed moderate interactions with some cytochrome P450 metabolizing enzymes.

* Corresponding author at: Department of Chemistry, Faculty of Physical and Computational Sciences, College of Science, Kwame Nkrumah University of Science and Technology, Kumasi, Ghana.
E-mail addresses: Akwasiacheampong.sci@knust.edu.gh (A. Acheampong), ikamponsah@knust.edu.gh (I.K. Amponsah).

https://doi.org/10.1016/j.sciaf.2024.e02455
Received 1 September 2024; Received in revised form 28 October 2024; Accepted 30 October 2024
Available online 30 October 2024

S. ataxacantha stem extract shows anti-plasmodial and antipyretic activities which may be due to its pentacyclic triterpenoid constituents inhibiting pfLDH.

Introduction

Malaria is a non-contagious life-threatening disease which is endemic in tropical regions of the world where the climatic conditions are conducive for the survival and transmissibility of the plasmodium parasite, the causative agent of the disease. In 2022, an estimated 249 million malaria cases were reported globally from 85 malaria endemic countries and claimed approximately 608,000 lives [1,2]. The WHO-African region recorded an estimated 233 million cases which was dominated by Nigeria, the Democratic Republic of the Congo, Uganda and Mozambique as the most endemic countries accounting for almost half of all cases globally [1]. The high prevalence and mortality rate of the disease in Sub-Saharan Africa is partly due to the habitable climate for the parasite and lack of healthcare facilities, compounded by frightening levels of poverty [3].

The World Health Organisation (WHO) had rolled out several preventive and interventional programs aimed at reducing the disease burden, especially in endemic countries, but despite these efforts, malaria remains a ubiquitous killer. The three main malaria control tools; nets, insecticides, and drugs have failed to yield the expected results in Sub-Saharan Africa [4]. The emergence of artemisinin partial resistance [5], and insufficient funds for malaria control and elimination have contributed towards this trend [6]. Also, malaria control programs, heavily based on insecticides, are unsustainable in poor countries. Another layer to this is the widespread and increasing resistance of mosquitos to pyrethroid-based vector control with higher costs of repurposed insecticides to address resistance [7]. Due to these factors together with the inaccessibility of healthcare facilities in sub-Saharan Africa, the majority of the populace in the region depend on the use of herbal medicines, which are readily available and cost-effective for the treatment of malaria [4].

The practice of using herbal medicines for the treatment of malaria has existed for thousands of years and has yielded the quinine and artemisinin derivatives used as modern antimalaria medicines [8]. For example, the isolation of the antimalaria aminoquinoline alkaloid quinine from the bark of *Cinchona* species became the template for the development of synthetic antimalarial drugs of the 4- and 8-aminoquinolines classes, such as chloroquine, primaquine, and amodiaquine. Similarly, clinically used antimalarial drugs such as artemether, dihydroartemisinin, and artesunate were developed from the sesquiterpene lactone artemisinin isolated from the leaves of the Chinese plant *Artemisia annua* [8,9,10]. However, the development of resistance to these conventional antimalaria drugs by the plasmodium parasite is a public health concern necessitating the urgent need for screening and development of new lead compound/s to mitigate the treatment of the disease [11]. Medicinal plants used in traditional medicine for the management of malaria remain a viable arsenal to explore in the search for novel drug candidates for malaria treatment.

Ghana is among 29 countries that accounted for 95 % of the global cases of malaria and contributed 3 % of global deaths due to the disease [6]. Most people use medicinal plants and their products (mostly polyherbal) documented in Ghanaian folklore medicine to manage the disease. The root of *Nauclea latifolia, Morinda lucida* (roots and leaves), *Azadirachta indica* (leaves), *Cymbopogon citratus* (leaves), *Picralima nitida* seeds (Ghana quinine), *Phyllanthus nuriri* (whole plant) and *Cryptolepis sanguinolenta* (roots), are the most popular antimalaria medicinal plants used in Ghanaian traditional medicine [12]. These plants have been widely investigated to exploit their antimalaria potential, including the isolation and structural elucidation of their antiplasmodial constituents [12,13,14]. However, there are several other plants that are also used by indigenous communities for malaria treatment but have not received much attention. An example is *Senegalia ataxacantha*, known locally as 'nwere'(Akan), is a scrambling woody shrub which is widely distributed in West and Southern Africa. There is overwhelming ethnomedical evidence from several countries on the use of the plant for abscesses, malaria, backache, cough, toothache, malaria, pneumonia, sores and wounds [15]. Pharmacological investigation of the plant validated the antibacterial, antifungal, antidiabetic, antioxidant and anti-inflammatory activities. Phytochemical investigation of the stem bark extract of the plant revealed the presence of betulinic acid, betulinic acid-3-trans-caffeate, lupeol and the chromene derivative acthaside [15,16,17]. The aim of this research was to give scientific credence to the use of the stem bark for malaria, track down the antimalaria constituents and elucidate the mechanism of anti-plasmodial activity using *in silico* studies. Molecular docking technique was selected to offer insights into the interactions between potential antimalarial compounds and their target proteins, thereby facilitating the rational design of efficacious drugs.

Materials and methods

Reagents, solvents, and equipment

Analytical grade solvents such as petroleum ether, ethyl acetate, ethanol and methanol were obtained from VWR chemicals BDH (France). DMSO, SYBR Green 1 (10,000 in DMSO), Immersion oil, and Giemsa stain were obtained from Sigma-Aldrich (Steinheim, Germany). Yeast powder was obtained from U.K. Chemicals (Kumasi, Ghana). Silica gel 70–230 mesh and aluminium precoated silica gel 60 F254 TLC plates were obtained from Merck KGaA (Darmstadt, Germany). Artesunate and acetaminophen were purchased from Phyto-Riker, Accra, Ghana. Equipment used included a Mettler Toledo electronic balance (ME204 ME, Vietnam), and oven (United Kingdom). Rotary evaporator (Stuart SRC4, COLE-PARMER Ltd.) obtained from the United Kingdom.

Plant material harvesting, authentication, and extraction

The stem bark of *Senegalia ataxacantha* was collected from Kwahu Asakraka in the Eastern Region of Ghana and was authenticated by Mr Cifford Asare of the Herbarium section of the Department of Herbal Medicine, Kwame Nkrumah University of Sciences and Technology (KNUST) (Voucher specimen number KNUST/HM1/2020/S002). The material was washed under running tap water, chopped into smaller pieces, and air dried at ambient temperature (28–35 °C) for 14 days. The dried plant material was coarsely powdered using a mechanical grinder, packed into brown paper bags and kept at the laboratory until required for use. Four (4) Kg of the coarsely powdered stem bark of *Senegalia ataxacantha* was Soxhlet extracted with 70 % ethanol and then concentrated under reduced pressure at 50 °C using the rotary evaporator. It was then dried on a water bath and kept in a desiccator (designated SA).

Isolation of constituents from the stem of senegalia ataxacantha

A weight of 60 g of the 70 % ethanol extract of SA was subjected to column chromatography on silica gel 60 (70–230 mesh) in a glass column. It was then eluted with gradient mixtures of petroleum ether, ethyl acetate (EtOAc), and ethanol (EtOH) to obtain 70 fractions (100 mL each). The fractions were bulked together by monitoring the chemical profiles with thin layer chromatography on precoated aluminium-backed silica gel plates 0.25 mm thickness. A total of seven bulk fractions designated B1–B7 were obtained (Fig. 1).

Fraction B2 (bulked from aliquot 6–11), which was a fatty solid (2 g), was washed with petroleum ether to obtain a white amorphous precipitate (1.2 g). The white precipitate was isocratically eluted with petroleum ether and ethyl acetate (ratio 98:2) on silica gel (70–230 mesh) to obtain 25 fractions of 25 mL aliquots. Sub-fractions 8 to 25 were bulked together and recrystallized in petroleum ether to obtain 400 mg of compound SA1. Bulk fraction B3 (1.3 g) was gradiently eluted with petroleum ether and ethyl acetate, starting with 100 % pet-ether up to pet ether/EtoAc (70:30), to afford four (4) bulk fractions labeled B3a to B3d. Sub-fraction B3a was very oily hence was not purified further. Sub-fraction B3b and B3c were bulked together, due to the similarity of the profiles, and eluted isocratically with pet ether/EtoAc (93:7) to afford compounds SA2 (0.2 g) as white crystals and SA3 (0.35 g) as a white amorphous powder. SA2 was found to be the same as SA1 by their physicochemical characteristics, co-chromatography on the TLC plate and by comparison of their infra -red spectra.

Bulk fraction B4 (1.3 g) was loaded onto a glass column containing silica gel 60 (70–230 mesh) and eluted with gradient mixtures of Pet ether/EtoAc starting with ratio 9:1 up to 3:2. The eluates were collected in 10 mL aliquots and bulked together according to their TLC profiles into four (4) sub fractions (B4a – B4d). Sub fraction B4b was washed with petroleum ether to yield SA4(0.2 g) as white amorphous powder. Sub fraction B4c was also recrystallised with 100 % petroleum ether to yield SA5 (0.35 g) as white amorphous powder.

Spectroscopic techniques

1D and 2D NMR spectra were recorded at 25 °C on a Bruker Adven 500 TM NMR spectrometer (Germany). Chemical shifts (δ) were expressed in parts per million (ppm) using tetramethyl silane (TMS) as an internal standard and coupling constants (J) were measured in Hertz (Hz). Functional groups were identified using the Bruker Fourier transform infrared (FT-IR) spectrometer scanned between 4000 and 400 cm^{-1} with a resolving power of 4 cm^{-1} and a cumulative scanning limitation of 24 times. A quadropole ion trap mass

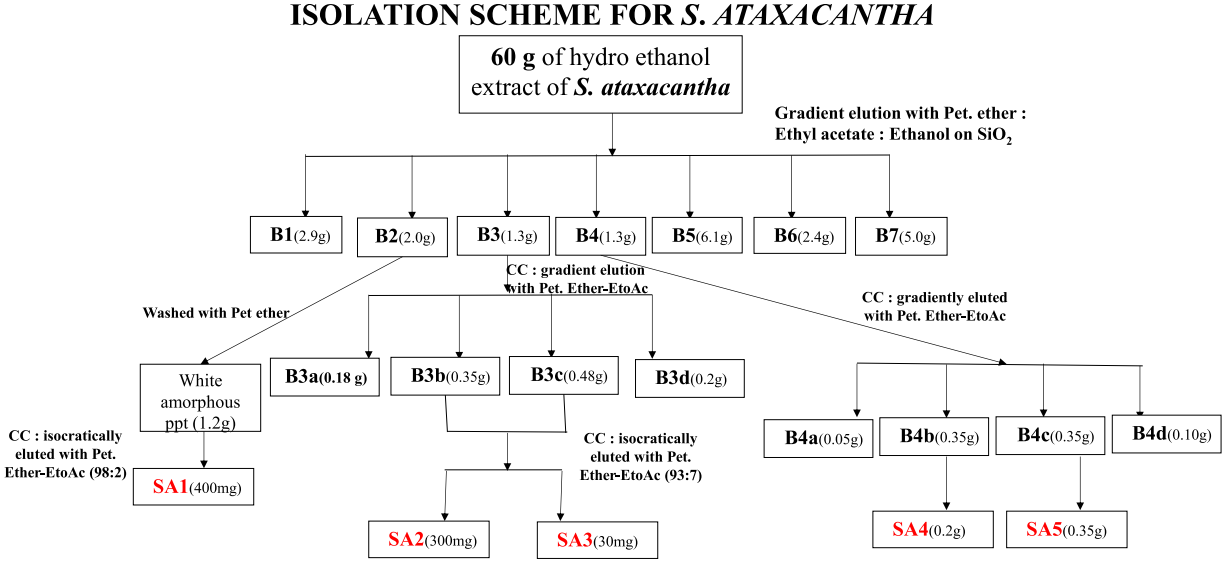

Fig. 1. Isolation scheme for the 70 % ethanol stem extract of *S. ataxacantha.*

spectrometer (Agilent 1100) equipped with an ESI source in the positive and negative ion mode and Xcalibur software Version 1.4 (Finningan) were used for data acquisition and processing.

Biological assays

Ethical clearance

Animal experimental techniques were conducted after the study received ethical permission from the Committee on Animal Ethics and Research, Department of Pharmacology, Kwame Nkrumah University of Science and Technology (KNUST/Cology/034). Furthermore, guidelines for the Helsinki Declaration for the care of experimental animals were meticulously observed [18].

Animals

Swiss albino mice and rats were obtained from Noguchi Memorial Institute for Medical Research (NMIMR), University of Ghana, Legon, Accra. Animals were kept and allowed to acclimatize at the animal house of the Department of Pharmacology, KNUST for a week before the start of the study. The experimental animal maintenance room was kept at a temperature of 24±1 °C, with relative humidity controlled within a range of 30 to 70 %. They were exposed to a 12:12 h dark-to-light cycle having unlimited access to quality drinking water and a pellet diet.

Acute toxicity

Senegalia ataxacantha has a long history of use in traditional medicine as an antimalarial plant without demonstrable toxicity hence the limit test at the single dose level of 3000 mg kg^{-1} body weight was adopted from the OECD Test Guideline 436 [19]. Swiss albino rats were put into two (2) groups of three (3). Animals were starved overnight and given water *ad libitum*. Following the starvation period, rats were weighed and dosed with 3000 mg kg^{-1} bodyweight of extract using an oral gavage. Feeding was delayed for another 3 h after drug administration, during which the rats were individually monitored at 30-minute intervals for the first 1 hour and then occasionally for 24 h, with specific attention paid to the first 4 h. Thereafter, observation was made daily for the next 13 days for indicators of toxicity including gross physical and behavioural changes.

Parasite inoculation

The ANKA strain of Plasmodium berghei (stored at −80 °C) was obtained from the KNUST Faculty of Pharmacy and Pharmaceutical Sciences (Department of Pharmacology). Healthy mice were infected with the Plasmodium parasite by intraperitoneal injection of 0.2 mL of inoculum (infected blood with the parasitaemia level: 1×10^7 parasitized erythrocytes) as described by Baah et al. [20].

Four-day suppressive antimalarial test

This test was used to evaluate the schizonticidal activity of the 70 % ethanol stem extract of *S. ataxacantha* against *P. berghei* infected mice [21]. Swiss Albino mice were inoculated on the first day (Day 0), intraperitoneally, with 0.2 mL of infected blood. They were then divided randomly into five groups of five mice per group. Three groups (II, III and IV) were assigned as test groups whereas groups (I & V) were used as negative and positive control respectively. Three hours post infection, 30, 100 and 300 mg kg^{-1}/day of 70 % ethanol extract (crude extract) of *S. ataxacantha* were administered to the test groups. Artesunate, at the dose of 4 mg kg^{-1}/day, and an equivalent volume of the vehicle (0.2 mL of 1 % tween 80 solution) were administered to the positive and negative control groups respectively, for four consecutive days (Day 0–3). On the fourth day (96 h post-infection), thin blood smears were prepared from the tails of each mouse. These smears were fixed with methanol and stained with 10 % Giemsa solution. Parasitaemia was assessed by counting the number of parasitized red blood cells among the total red blood cells in five randomly chosen fields on the slide, using a light microscope (Leica DM750, Wetzlar-Germany). The percentage parasitaemia was calculated as described by Baah et al. [20].

Rane's curative test

The curative potential of the stem extract of SA was evaluated following the method described by Nardos et al. [22]. Seventy-two (72) hours after parasite inoculation, mice were randomly divided into five groups, with the establishment of parasitaemia confirmed. These groups were administered 30, 100 and 300 mg kg^{-1}/day of the extract, 4 mg kg^{-1}/day of artesunate or 2 mL/day of the vehicle, for 4 consecutive days. Thin blood smears were taken from the tail vein of each mouse before treatment and 24 h after the final treatment to assess parasitaemia. Body weights were recorded prior to treatment and again on day 7 post-infection.

Antipyretic activity of S. ataxacantha

The antipyretic potential of the hydroethanol stem extract of *S. ataxacantha* was assessed using the yeast-induced pyrexia (pathogenic fever) [22,23,24]. Swiss albino rats, both male and female, were separated into five groups and starved overnight with unlimited access to water. Baseline rectal temperatures were measured for each rat using a digital thermometer. Pyrexia was induced by subcutaneous injection of a 30% w/v yeast powder solution in 0.9 % normal saline solution beneath the nape of the neck. Rectal temperatures for each rat were recorded 18 h post yeast administration, a point at which fever reaches a steady plateau phase. The positive control group (group V) received the standard drug (100 mg kg^{-1} Acetaminophen), the vehicle control (group I) received 10 ml/kg normal saline while the extract-treated groups received 30 mg kg^{-1} (group II), 100 mg kg^{-1} (group III) and 300 mg kg^{-1} (group IV). The extract and standard drug were administered orally via gavage. Temperatures were measured at 1, 2, 3, and 4 h after dosing. The percentage reduction in rectal temperature was calculated following the method described by Yimer et al. [25].

In vitro antiplasmodial activity of isolated compounds

The isolated compounds were assessed for their *in vitro* antiplasmodial activity using the SYBR green I fluorescence assay [26] against chloroquine-sensitive (3D7) and chloroquine-resistant (Dd2) strains. Stock concentrations of the compounds at 10 mg/ml, were diluted with culture media to a concentration of 100 ug/mL. Test concentrations for the compounds and reference drug artesunate were prepared using a two-fold dilution at 9 dose levels ranging from 100 to 0.39 ug/mL. Each test well received 90 μL of ring-stage parasitized blood (pRBCs) with a haematocrit of 2 % and parasitaemia of 1 %. An additional 10 μL of the various test drug concentrations was then added to their corresponding wells. The experiments were conducted in triplicate, with negative control containing no drug. The plates were incubated at 37 °C in a candle jar for 48 h. Following the incubation period, 100 μL of SYBR green I (in lysis buffer) added to each well, and the plates were incubated for an additional 30 min at room temperature. Absorbance was measured using a multi-well plate reader (Guava easycyte HT FACS machine, Millipore, USA) with excitation and emission wavelength set at 485 nm and 530 nm, respectively. The half-maximal inhibitory concentration (IC_{50}) was calculated using GraphPad Prism software.

Statistical analysis

Data analysis was done using Graph Pad Prism. (GraphPad Software version 9.1.5, San Diego, CA, USA). Comparisons were made against negative controls as well as among treatment groups using a one-way analysis of variance (ANOVA) followed by the Dunnett's multiple comparison tests. Body weights changes were compared using two-way ANOVA followed by Dunnett's multiple comparison tests. The results were considered significant statistically at 95 % confidence level. The concentration that inhibits asexual *Plasmodium falciparum* parasite by 50 % (IC50) were determined from dose-response curves by non-linear regression analysis using Graph pad Prism version 9.1.5. Software.

In silico studies on isolated compounds

Molecular docking was performed to investigate the interactions of the isolated compounds friedelin, friedelinol, lupeol, and sitosterol with parasite lactate dehydrogenase (*pf*LDH), aiming to explore their antimalarial properties. Chloroquine, a known antimalarial drug, served as a reference.

Target protein retrieval

In this study, we investigated the interaction between four compounds isolated from the stem of *S. ataxacantha* and *pf*LDH enzyme with PDB ID 2 × 8l The three-dimensional (3D) structures of the selected compounds were obtained from public databases, including PubChem and DrugBank [27]. The 3D structure of *pf*LDH (PDB ID: 2 × 8l) was retrieved from the Protein Data Bank (PDB) [28]. The interactions of 2 × 8l with glycerol were visualized using LIGPLOT, a tool from the PDBSUM pictorial database [29]. To prepare the 2 × 8l structure for docking analysis, all water molecules and bound glycerol were removed, and hydrogen atoms were added using Discovery Studio Visualizer. The prepared structure was then saved for subsequent docking analysis (Fig. 2).

Blind docking with Swiss dock

To investigate the molecular interaction between the isolated compounds and *pf*LDH, blind docking was performed using the SwissDock server (http://www.swissdock.ch/) [30]. The docking was set to the accurate mode, with no flexibility allowed for the side chains of any amino acid in the target protein. Additionally, a specific binding pocket was not predefined to avoid biasing the docking

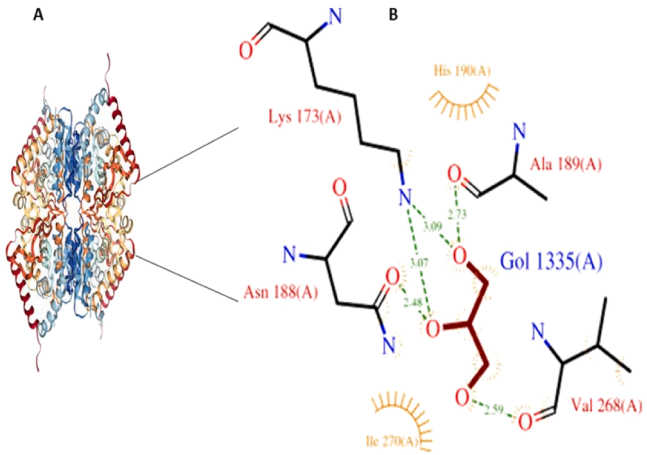

Fig. 2. Cartoon (A) and LIGPLOT (B) representations of the pf-LDH protein. The LIGPLOT shows the interaction of the protein with glycerol.

toward a particular active site. The protein structure was uploaded as a PDB file, while the compounds were provided as Mol2 files. SwissDock generated all possible binding modes for each ligand, clustering the most favourable ones according to their interactions within given pockets. The output from SwissDock, referred to as the "prediction file," contained information on cluster rank, number of elements in each cluster, full fitness score, and estimated binding free energy (ΔG). A cluster represents a potential binding pocket on the target protein, with each cluster rank indicating different conformations of a ligand within that pocket. Typically, the model with the lowest energy in cluster zero is considered the most favourable for interaction.

Clusters visualization

After docking, Chimera software, Protein-Ligand interaction profiler (https://plip-tool.biotec.tu-dresden.de/plip-web/plip/result/7eef0918-fee5–4125-a143-bb2dddc98ade) [31] and PDBSUM was used to visualize the receptor ligand interactions for the lowest energy model of the clusters obtained from the previous step. Each ligand cluster was inspected for amino acids interacting with the

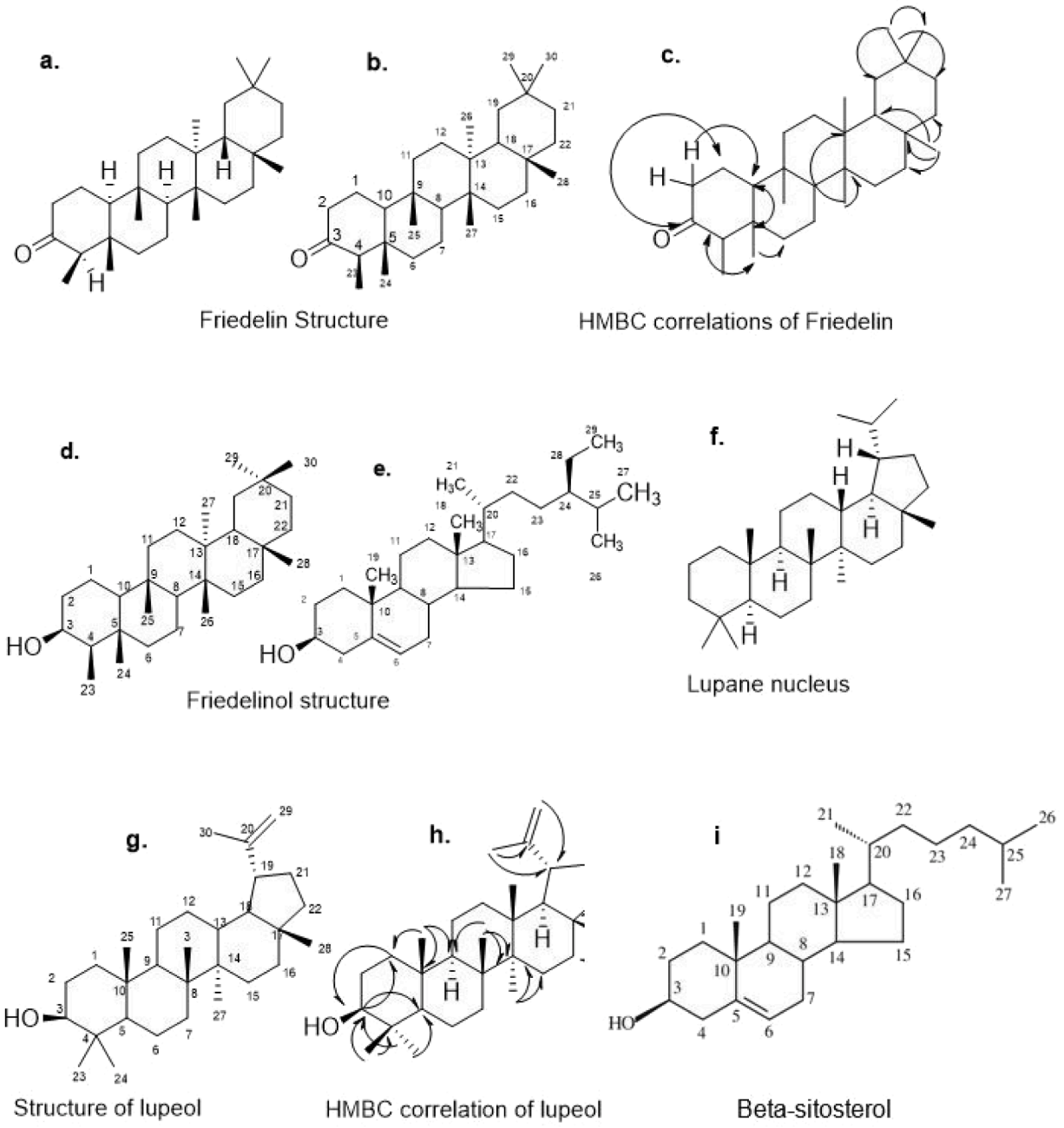

Fig. 3. Pentacyclic triterpenoids from the stems of *Senegalia ataxacantha*.

ligand, hydrogen bonds (H-bonds) and the specific atoms involved. All the interacting amino acids with the target were noted for each cluster.

Drug likeliness, pharmacokinetic and oral toxicity evaluations

To analyse drug likeliness and the pharmacokinetics parameters, all the molecules were subjected to ADMET (Absorption, distribution, metabolism, excretion and toxicity) predictions with Swiss ADME (http://www.swissadme.ch/) [32] and PROTOX web servers (http://tox.charite.de/protox_II/) [33]. PROTOX predicts the median oral lethal dose, LD50 (Lethal dose, 50 %) based on the analysis of the two-dimensional similarity to compounds with known LD50 values and the identification of fragments over-represented in toxic compounds.

Results and discussion

Structural elucidation of compounds

Elucidation of the structure of compound SA1/SA2

SA1/SA2 was isolated as a white crystalline solid soluble in chloroform. It gave a positive reaction to Salkowski's test for triterpenoids. The IR spectrum (Supplementary file 1) showed characteristic absorption bands at V_{max} of 2926.91 and 2868.93 (C—H stretch) and 1713.12 (C = O) cm^{-1}. There were no absorption bands for hydroxyl (OH) or C = C functionalities. The ^{1}H NMR spectrum (Table 1; Supplementary file 2) revealed upfield resonance signals for 7 methyl singlets at δ 0.72 (Me-24), 0.87 (Me-25), 1.01 (Me-26), 1.05 (Me-27), 1.18 (Me-28), 1.0 (Me-29) and 0.94 ppm (Me-30) and another methyl group appearing as a doublet at δ 0.88 ($J = 4.56$, Me-23) due to coupling with the methine proton at δ 2.25. The cluster of signals enveloped between δ 0.7 to 2.39 ppm was consisted with the presence of methine, methylene and methyl protons of triterpenoid skeleton(Fig. 3A-C) [34].

The ^{13}C NMR spectra (Table 2; Supplementary file 2) displayed 30 resonance signals for seven (7) quaternary, four (4) methine, eleven (11) methylene and eight (8) methyl carbons typical of the friedelane pentacyclic triterpenoids [34,35]. The eight methyl signals occurred at δ 7.1 (C-23), 14.9 (C-24), 18.5 (C-25), 20.5 (C-26), 18.9 (C-27), 32.1 (C-28), 35.3 (C-29) and 32.0 ppm (C-30). The downfield signal at 213 ppm depicted the presence of the carbonyl functionality, as observed in the FT-IR spectrum of the compound. The HSQC spectrum of SA1 showed correlation between C-4 and the signal integrating for one proton at δ 2.25 ppm (H-4). Similar correlations were found between C-8 with δ H 1.38, C-10 with δ_H 1.53, C-18 with δ_H 1.56 and C-24 with δ_H 0.72 ppm. In the HMBC spectra, the methyl protons at δ 0.88 ppm (H-23) showed long range correlation with C-5 (δ 37.8.0 ppm) and C-3 (δ 213.2 ppm) (Fig. 3C). Similarly, the methylene protons at δ 2.37 (H-2) showed HMBC correlation with C-4 and the carbonyl signal C-3 (Supplementary file 2). All the resonance positions of the carbon and proton NMR agreed with that published for friedelin [34] . This was confirmed by the molecular ion peak of 426 in the mass spectrum (Figure S1), which was consistent with the formular for friedelin ($C_{30}H_{52}O$). This is the first report of the isolation of friedelin from *Senegalia ataxacantha*.

Characterisation of compound SA3 as a mixture of friedelin and friedelinol

SA3 was isolated as a white amorphous powder, soluble in chloroform with a melting point of 282–296 °C. It gave a positive reaction to the Salkowski test for triterpenoids. The IR spectrum showed absorption bands (V_{max}) for hydroxyl functionality at 3375.84, carbonyl at 1707.78, and others at 2930.73, 2868.0, 1454.07 and 1383.77 cm^{-1}. The IR spectra of SA3 differed from SA1 by the presence of the hydroxyl (OH) group in the former (Fig. 3D-E; Supplementary file 1)

The ^{1}H NMR spectra (Table 1; Supplementary file 3) showed signals that were consistent with those reported for compound SA1 except for a doublet at δ 3.73 ppm integrating for one proton assignable to the methine proton of the carbinol group as suggested by the IR data. Additionally. the methine and methylene protons at C-4 and C-2 shifted upfield to δ1.25 and 1.96 ppm respectively due to the replacement of the highly deshielding carbonyl group in SA1 with the hydroxyl group in SA3. The methyl envelope between δ1.25 and 0.72 ppm revealed several overlapping singlets and a doublet consistent with the eight methyl signals of SA1 suggesting that SA3 may contain SA1. This was confirmed in the ^{13}C NMR spectrum, which displayed carbon resonances consistent with compound SA1 with some additional signals. Notable additions included the carbinol signal at δ 72.89 (C-3), 61.48 (C-10), and the upfield shift of C-4 and C-2 to δ 49.3 and 36.2 ppm respectively. The replacement of the highly deshielding C = O (in friedelin) with a hydroxyl group at C-3, thereby shifting the resonance positions of the surrounding atoms (C-2 and C-4) upfield is consistent with the presence of friedelinol, a structural analogue of friedelin [36,37]. A weak carbonyl signal at δ213.46 ppm confirmed the C = O functionality of friedelin (Fig. 3). These observations confirmed SA3 as a mixture of friedelin and friedelinol. Due to the structural similarity of friedelin and friedelinol, some of the carbon signals overlapped, with others resonating at the same chemical shift as seen in the intensity of the signals whereas others differed by δ±0.2ppm. The mass spectrum of SA3 (Figure S1), however, showed the sodium and potassium adduct molecular ions 449 and 465 respectively consistent with friedelin. The absence of the molecular ion peak for friedelin could be due to its concentration in the mixture. Several reports have shown that friedelin and friedelinol are often isolated as a mixture [38,39]. This is the first report of the occurrence of 3β-friedelinol in the stems of *Senegalia ataxacantha*.

Structural elucidation of compound SA4 as β-sitosterol

Compound SA4 was isolated as a white amorphous solid with a melting point of 135–141 °C. It also gave a positive reaction to triterpenoids in the Salkowski's test. The IR spectrum (Supplementary file 1) displayed absorptions bands (V_{max} cm^{-1}) for a germinal dimethyl group (-$CH_3(CH_3)$2) at 1367.19 and a weak unconjugated olefinic C = C vibration at 1666.90. Other absorption bands appeared at 2935.12 and 2865.76 cm^{-1} (C—H absorption), cyclic methylene C—H stretches at 1463.78 and a weak band at 3348.17

cm^{-1} attributed to the OH group. The FTIR spectrum of compound SA4 was consistent with that published for β-sitosterol [40] (Table 1).

Further confirmation from the ^{1}H NMR spectrum (Supplementary file 4) included a multiplet integrating for one proton assignable to the proton attached to the carbinol (-C-OH) group at δ 3.52 ppm. Similarly, the olefinic proton signal occurred as a doublet at δ 5.35 ppm. Two methyl singlets occurring at δ 0.68 and 1.05 ppm were assigned to the angular methyl groups attached to the quaternary carbons C-18 and C-19 respectively. Four other methyl groups resonated at δ 0.82, 0.84, 0.86 and 0.92 ppm. The multiplets at δ 2.28 and 2.0 ppm integrating for two protons each were assigned to the two methylene protons adjacent to the carbinol group. The assignment of the proton signals in the spectrum of SA2 agreed with that published by Ododo et al. [40] and Aliba et al. [41] for β-sitosterol (Fig. 3I).

The ^{13}C NMR spectrum (Table 3; Supplementary file 3) revealed 29 resonance signals with the chemical shift at δ 140.77 and 121.68 ppm elaborating the olefinic carbons at C-5 and C-6 respectively. The signal at δ 71.96 ppm was assigned to the carbinol group (-C-OH) at C-3. The olefinic group and hydroxyl functionalities corroborated the findings in the IR spectrum. Six methyl groups occurred at δ 12.01 (C-18), 19.97 (C-19), 18.89 (C-21), 19.55 (C-26), 19.18 (C-27) and 12.13 (C-29) ppm. The signals at C-18 and C-19 were assigned to the angular methyl carbons with the former resonating more upfield due to the γ-gauche interaction that increases the screening of the C18. However, the deshielding effect of the olefinic group on C-19 made it resonate at a higher frequency. The mass spectrum (Figure S1) of compound SA4 showed a molecular ion peak at *m/z* of 414.3521 which agreed with that of β-sitosterol with a molecular formular of $C_{29}H_{50}O$ (calculated molecular weight of 414.258). All the spectra data, including the HSQC, HMBC and COSY experiment (Supplementary file 4) agreed with that published for β-sitosterol [39,40].

Characterisation of SA5 as lupeol

Compound SA5 was isolated as a white amorphous powder and responded positively to the triterpenoid test by the formation of a reddish-brown ring at the junction of the chloroform- concentrated H_2SO_4 mixture. The ^{1}H NMR (Supplementary file 5) showed the presence of a hydroxy group attached to C-3 at δ 3.18 ppm (IH, dd). The olefinic geminal methylene protons at δ 4.68 (C-29a) and 4.56 (C-29b) as well as the methyl singlet at 1.68 ppm (C-30) confirmed the lup-20(29)-ene system. The cluster of signals between 0 and 2 ppm was due to the overlapping methyl, methylene and methine envelope consistent with the steroidal nuclei. These were corroborated by the Fourier transform infra-red spectra (FTIR) (Supplementary file 1) which displayed the hydrogen bonded OH stretch at an absorption of 3324.48 cm^{-1}, the C = C symmetric stretch of the olefinic moiety at 1637 cm^{-1}, =C—H exocyclic bonding CH_2 at 878.97 and C—O stretch absorption band of a secondary alcohol at 1041.74 $cm^{-}1$. Others included C—H stretch in CH_3 and CH_2 absorbing at 2872.02 and 2943.40 cm^{-1} respectively.

The ^{13}C NMR (Table 3) displayed carbon signals which was consistent with the 30-carbon skeleton of pentacyclic triterpenoids [42]. The olefinic signals at δ 109.47 and 151.09 ppm, assigned to C-29 and C-20 respectively, together with the 7 methyl groups confirmed the existence of the lup-20(29)-ene system [43] (Fig. 3F-H). The deshielded oxymethine signal at δ 79.59 ppm was assigned to C-3, confirming the presence of OH group as suggested by the FTIR spectrum. The HSQC spectrum showed some important cross peaks between the hydroxy proton at δ 3.18 ppm and C-3 (δ 79.59 ppm), methylene protons at δ 4.68/4.56 ppm and C-29 (δ 109.47). The signal integrating for 3 protons at δ 1.68 showed long range correlations with C-19 (J^3), C-20 (J^2), and C-29 (J^3). The correlation of the methine proton at δ 2.37 (H-19) with C-20 and C-30 showed that the isopropenyl chain was attached to the pentacyclic nucleus at C-19 (Fig. 3H). This was corroborated by the J^3 correlations of the germinal proton at δ 4.68 with C-19 and C-30. Other HMBC correlations occurred between H-25(0.83) and C-5 (55.49), C-9 (50.62) and C-4 (38.89); H- 28 (0.79) and C-18 (48.49), C-16 (35.76) and C-17 (43.16); H-23 (0.97) and C-3 (79.59), C-5 (55.49), C-4 (38.89), and C-24 (15.52); H-24 (0.76) and C-3 (79.59), C-5 (55.49), C-4 (38.89) and C-2 (27.59). The spectra data presented and the melting point of compound SA5 (215 −216 °C) agreed with that published for lupeol [44] with molecular formular $C_{30}H_{50}O$. The index of hydrogen deficiency was calculated to be equal to 6 which agreed with the pentacyclic ring structure and the exocyclic olefinic group. Lupeol has been reported from the stem bark of *Senegalia ataxacantha* and other species of the genus Acacia [15,16].

Table 1
Key 1H—NMR resonance signals of compound SA1, SA3, friedelin and friedelinol.

Number of Carbons	δ ^{1}H NMR of SA1	δ ^{1}H NMR of SA3	δ ^{1}H NMR of Friedelin*	δ ^{1}H NMR of Friedelinol^
H-1	1.96 m	1.53	1.95 m	1.58 m
H-2	2.39 m	2.26	2.37 ddd	2.16 q
H-3	–	3.73	–	3.41
H-4	2.26	1.17	2.25q	1.17
"	"	"	"	"
"	"	"	"	"
23	0.88 (3H, d)	0.86(3H, d)	0.88	1.01 (d)
24	0.72 (3H)	0.72	0.73	0.78
25	0.87 (3H)	0.87	0.87	0.81
26	1.01 (3H)	0.99	1.01	0.98
27	1.05(3H)	1.05	1.05	1.01
28	1.18 (3H)	1.17	1.18	1.18
29	1.0 (3H)	0.96	1.0	0.97
30	0.95 (3H)	0.93	0.94	1.02

Ambarwati et al. [34], ^Salazar et al. [37].

Table 2
^{13}C NMR spectra of SA1, SA3, friedelin and friedelinol.

Number of Carbons	δ ^{1}C NMR of SA1(500 MHz, $CDCl_3$)	δ ^{1}C NMR of Friedelin* (500 MHz, $CDCl_3$)	δ ^{1}C NMR of SA3 (500 MHz, $CDCl_3$)	δ ^{1}C NMR of Friedelinol^ (500 MHz, $CDCl_3$)
1	22.5	22.3	22.4/16.5	16.2
2	41.5	41.5	41.4/36.2	36.1
3	213.2	213.2	213.5/72.9	71.6
4	58.4	58.2	49.3	49.6
5	42.4	42.1	42.3/38.4	38.1
6	41.8	41.3	41.9/41.9	41.99
7	18.2	18.2	18.1/17.7	17.7
8	53.3	53.1	53.3/53.3	53.3
9	37.7	37.4	37.6/37.2	37.2
10	59.7	59.5	59.6/61.5	61.7
11	35.8	35.7	35.8/35.7	35.7
12	30.7	30.5	30.8/30.7	30.7
13	39.9	39.7	39.8/38.5	38.4
14	38.5	38.3	38.0/39.8	39.7
15	32.6	32.4	32.6/32.9	32.3
16	36.2	36	36.2/36.2	35.9
17	30.2	30	30.1/30.1	30.0
18	43.	42.8	43.0/42.9	42.8
19	35.6	35.3	35.3/35.3	35.4
20	28.4	28.2	28.3/28.3	28.2
21	32.9	32.8	32.9/33.0	32.9
22	39.5	39.2	39.4/39.4	39.3
23	7.1	7	7.0/11.8	12.1
24	14.9	14.6	14.8/15.9	16.6
25	18.5	17.9	18.4/18.4	18.4
26	20.5	20.2	20.4/20.3	20.1
27	18.9	18.6	18.8/18.8	18.7
28	32.1	32.1	32.2/32.2	32.1
29	35.3	35	35.3/35.2	35.0
30	32.0	31.8	32.1/31.9	31.9

* Ambarwati et al. [34]., ^Salazar et al. [37].

Acute oral toxicity

Administration of the 70 % ethanol extract of the stem bark of *S. ataxacantha* (SA) at a dose of 3000 mg kg^{-1} did not result in any observable physical or behavioural changes within 24 h, and no mortality occurred during the subsequent 2-week observation period. This indicates that the extract has a high margin of safety, with the estimated LD_{50} being above 3000 mg kg^{-1}. These findings lend support to the traditional use of *S. ataxacantha* for treating various ailments without apparent toxicity. These results are in line with other studies showing a low toxicity profile for different parts of the *S. ataxacantha* plant. Amoussa et al. [45] found that oral administration of 2000 mg kg^{-1} did not cause significant alterations in hematological and biochemical parameters or damage to liver and kidney tissues. Akapa et al. [46] similarly estimated the LD_{50} for the methanol leaf extract to be greater than 5000 mg kg^{-1}, reinforcing the notion of a broad safety margin. It's worth noting that acute toxicity tests provide initial safety data, generally covering a shorter observation period that aligns with typical malaria treatments, which are often under seven days. However, to ensure a comprehensive safety profile, sub-acute toxicity testing is recommended. This is especially important because herbal products are frequently self-administered in many regions where malaria is endemic [47], often without medical supervision. Sub-acute testing helps to assess potential long-term effects or cumulative impacts on organ functions, offering a more complete understanding of the extract's safety.

Antiplasmodial activity

SA significantly ($p < 0.05$) reduced parasitaemia at all tested doses in both suppressive and curative studies (Table 4). SA also exhibited a dose-dependent suppression of parasites in both assays, with the highest suppression rates of 63.39 % and 63.32 % observed in the suppressive and curative tests, respectively. In all groups, except the 300 mg kg^{-1} group, SA demonstrated greater suppression in the suppressive assay compared to the curative assay. However, artesunate, the reference drug, achieved a higher rate in both the suppressive (63.80 %) and curative (85.25 %) assays compared to SA (Table 4).

Peter's 4-day suppressive assay is commonly used as a preliminary model to evaluate the antimalarial activity of potential compounds against *Plasmodium berghei* [48]. This assay examines the ability of a treatment to inhibit the initial proliferation of parasites, which may include both direct antiparasitic effects and the stimulation of the host's immune response [49]. The curative assay, on the other hand, measures a compound's effectiveness in clearing established parasitic infections [20], simulating the typical state in which plant-based remedies are used to treat malaria in endemic regions. The stronger suppressive effect of SA in the early stages of infection suggests it may be most effective when malaria is detected early. According to the classification system by Muñoz et al. [50], *Senegalia*

Table 3
C—NMR spectral data of compound SA2, SA3, sitosterol and lupeol.

Position	δ ^{13}C NMR of SA5 (ppm)	δ ^{13}C of Lupeol*(ppm)	δ ^{1}C NMR of SA4(500 MHz, $CDCl_3$)	δ ^{1}C NMR of β-sitosterol^ (400 MHz, $CDCl_3$)
C-1	38.24	38.08	37.40	37.28
C-2	27.59	27.43	21.23	21.69
C-3	79.59	79.05	71.96	71.82
C-4	38.89	38.73	42.48	42.33
C-5	55.49	55.33	140.77	140.77
C-6	18.49	18.34	121.68	121.73
C-7	34.47	34.31	32.04	31.93
C-8	41.01	40.89	31.81	31.93
C-9	50.62	50.47	50.28	50.16
C-10	37.34	37.20	36.73	36.51
C-11	21.11	20.95	21.23	21.11
C-12	25.33	25.17	39.93	39.80
C-13	39.02	38.88	43.61	42.34
C-14	43.00	42.86	56.92	56.79
C-15	27.62	27.47	24.50	24.33
C-16	35.76	35.61	28.44	28.27
C-17	43.16	43.02	56.22	56.08
C-18	48.49	48.34	12.01	11.89
C-19	48.15	48.00	19.97	19.42
C-20	151.09	150.98	36.34	36.17
C-21	30.03	29.87	18.89	18.84
C-22	40.17	40.02	34.05	33.98
C-23	28.13	28.00	26.21	26.11
C-24	15.52	15.37	45.99	45.86
C-25	16.27	16.13	29.30	29.19
C-26	16.15	16.00	19.55	19.84
C-27	14.71	14.57	19.18	19.06
C-28	18.16	18.02	23.21	23.10
C-29	109.47	109.33	12.13	12.01
C-30	19.47	19.32		

* Mailafiya et al. [44], ^Ododo et al. [40].

Table 4
Suppressive and curative activities of the extracts on *P. berghei*-infected mice.

	Suppressive			Curative	
Dose (mg kg^{-1})	% Pst	% SUPP	% Pst DAY 3	DAY 7	% SUPP
NC	45.00 ± 5.21	NS	52.00±5.21	56.00±5.21	NS
300	16.47 ± 5.72*	63.39	50.68±6.45	20.54±4.41*	63.32
100	24.77 ± 2.82*	44.95	56.84±5.85	28.15±5.08*	49.73
30	33.65 ± 0.93*	25.22	54.16±7.04	33.93±5.21*	39.41
PC (4)	16.29 ± 2.67*	63.80	54.47±3.78	8.26±0.52*	85.25

Values are presented as Mean±SD, $N = 5$, NC = vehicle-treated group, ART = Artesunate,%Pst = Percentage parasitaemia, NS = No Suppression, SUPP= Suppression. *Values are significantly different at $p < 0.05$ compared to NC.

ataxacantha can be considered to have good antiplasmodial activity in both the suppressive and curative assays.

Treatment with SA also prevented significant weight loss in mice compared to the vehicle-treated group (Fig. 4), suggesting a protective effect against some of the deleterious symptoms of malaria. Artesunate-treated mice also maintained their body weight. In the curative assay, SA demonstrated a dose-dependent protective effect against weight loss, indicating its potential to mitigate the severe symptoms of malaria which could lead to increased mortality [20]. Weight loss in malaria is a key concern because it can exacerbate the disease's pathology and potentially lead to death. These results support further exploration of *Senegalia ataxacantha* as a potential antimalarial treatment, with a particular focus on its effectiveness in the early stages of infection and its role in alleviating some of the severe symptoms associated with malaria.

A supplementary *in vitro* antiplasmodial assay of the extract and the isolated compounds (triterpenoids) corroborated the findings in the *in vivo* assay. The crude extract of *S. ataxacantha* showed higher activity than the isolated compounds but was over 7000 and 100-fold less potent than artesunate (reference drug) when used against the 3D7 and Dd2 strain respectively (Table 5). The triterpenoids were less potent than the crude extract. It could be that the main anti-plasmodial compound in the plant was not isolated since the polar fractions from the chromatographic fractionation were not purified due to resource constraints. It could also be inferred that the triterpenoids worked in synergy to establish the observed activity in the crude extract. The order of anti-plasmodial activity of the terpenoids was lupeol>friedelin/friedelinol mixture>friedelin>β-sitosterol. The result agrees with several reports of the anti-plasmodial activity of these compounds.

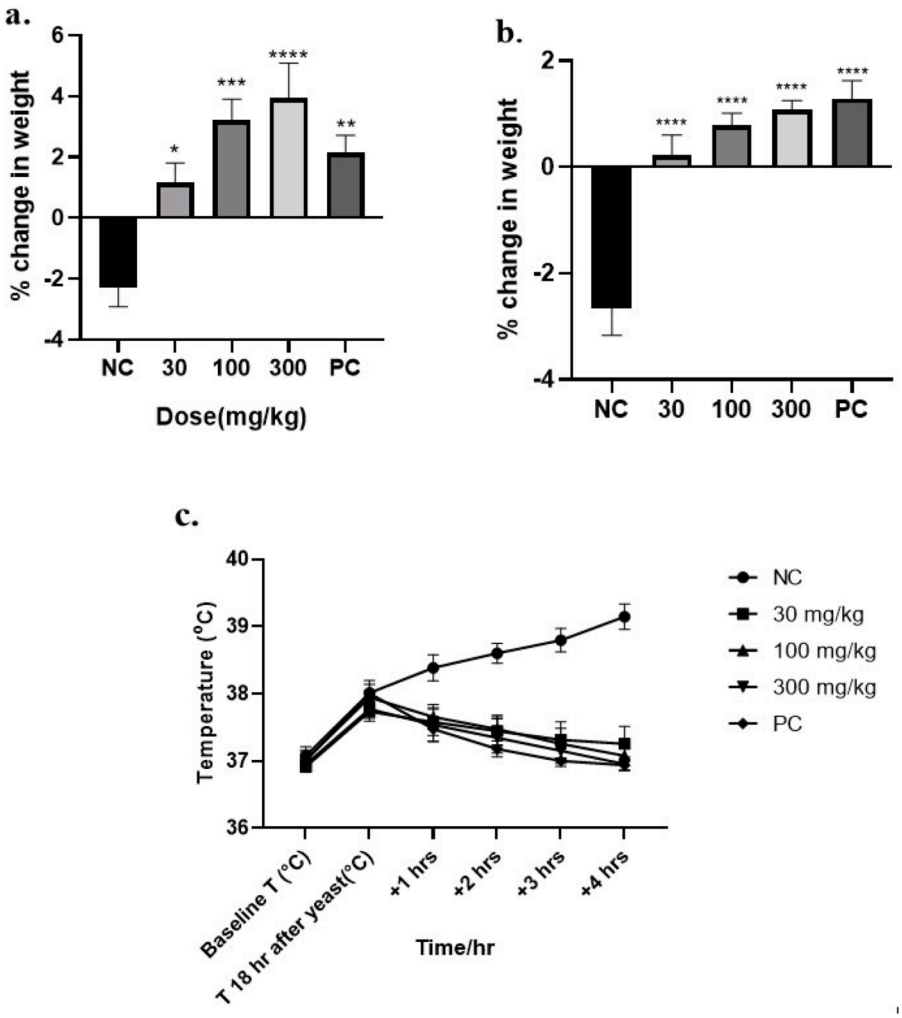

Fig. 4. Percentage change in weight of mice infected with *P. berghei* before and after treatment in the suppressive (A) and curative (B) assay. Change in rectal temperature of yeast induced rats (C) Values are significantly different at $^{*}p < 0.05$, $^{**}p < 0.005$, $^{***}p < 0.0005$, $^{****}p < 0.0005$ compared to the untreated group (NC).

Table 5
In vitro antiplasmodial activity of *S. ataxacantha* stem extract and isolated triterpenoids against 3D7 and Dd2 *F. falciparum* strains.

Extract/compounds	IC_{50} 3D7 (μg/mL)±SD	IC_{50} Dd2 (μg/mL)±SD
SAE	30.15±2.43	52.43±3.98
Friedelin	175.43±6.24	264.58±4.34
Friedelinol/Friedelin mixture	66.31±1.32	102.44±5.57
Sitosterol	280.32±4.85	>300
Lupeol	52.4 ± 6.74	80.32±2.33
Artesunate	0.0042±0.00	0.48±0.03

3D7: *P. falciparum* chloroquine sensitive strain; Dd2: *P. falciparum* chloroquine resistant strain.

Friedelin, unlike its reduced product 3β-friedelinol, is widely distributed in plants [20,39,51]. Friedelin, isolated from *Allanblackia gabonensis* leaves showed antiplasmodial efficacy against chloroquine-sensitive F32 and resistant FcM29 strains, respectively, with IC_{50} (μM) values of >200 and 145.8 respectively [52]. This validates and bolsters the potential of the compound and the plant extract as antimalarial agents. The mixture of friedelinol and friedelin showed higher activity than friedelin alone. Lupeol, was previously isolated from S. *ataxacantha* [17], and also from the leaves of *Ficus benjamina* [16,53]. It has been found to exhibit significant anti-plasmodial activity. A study conducted by Singh et al. [53] demonstrated lupeol's anti-plasmodial activity with an IC_{50} of 3.8 μg/ml against 3D7 Plasmodium strains. Similarly, the ubiquitous phytosterol β-sitosterol, has been reported to have inhibitory effects

on the growth of *Plasmodium falciparum* K1 strain with an IC_{50} of 45.00 μM [54]. Our results, however, did not show marked antiplasmoidal activity. These compounds may have contributed to the antiplasmodial activity of the hydroethanolic stem extract of *S. ataxacantha.*

Antipyretic activity of S. ataxancatha

The hydro ethanol stem extract of *S. ataxacantha* generally exhibited *in vivo* antipyretic activity in rats, which was evidenced by a significant ($p < 0.05$) reduction in rectal temperature against yeast-induced fever (Fig. 4C). After four hours of treatment, the groups of Swiss albino rats that received acetaminophen (100 mg kg^{-1} body weight) and the extract (30, 100 and 300 mg kg^{-1} body weight) lowered the rectal temperature by 2.8 %, 1.27 %, 2.34 % and 2.24 % respectively. However, there was no significant difference between the treated groups.

Yeast-induced pyrexia, also known as pathogenic fever, was used to assess the antipyretic properties of *S. ataxacantha's* hydro ethanol stem extract. Pyrexia is characterized as a complex physiological reaction brought on by an aseptic stimulus or an infection.

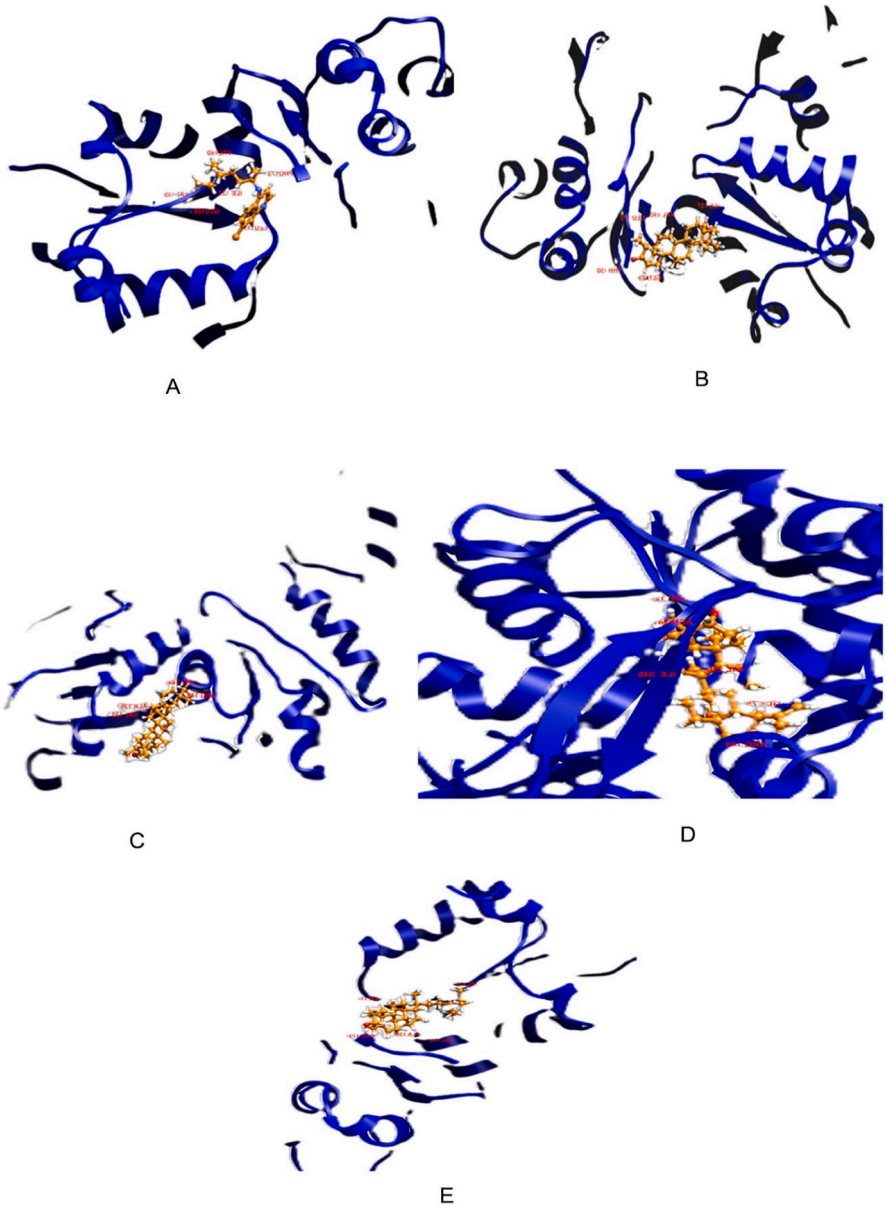

Fig. 5. Docking poses of the studied compounds alongside the corresponding amino acid residues within the binding site residues of the 2 × 8l protein structure. A: Chloroquine; B: Friedelin; C: Fredelinol, D: Lupeol; and E. Sitosterol.

PGE2 builds up in the pre-optic area of the hypothalamus, which elevates body temperature. Increased PGE2 production often modifies the hypothalamic neurons firing rate, which regulates thermoregulation.

Most antipyretic medications are believed to exert their effects by inhibiting the cyclooxygenase (COX) enzyme, leading to a reduction in prostaglandin E2 (PGE2) levels in the hypothalamus, which helps lower fever [55]. However, other mechanisms could also play a role in treating pyrexia, and they should not be discounted. It's interesting to note that a previous study by Abbas et al. [56] examining the antipyretic activity of the methanolic leaf extract of *S. ataxacantha* found no significant results. This discrepancy could be due to differences in phytochemical composition across various plant parts, highlighting the importance of considering the specific source of plant-based extracts when investigating their therapeutic properties.

The compounds isolated from the plant might have contributed to the antipyretic activity of the plant. Antonisamy et al. [57] showed that friedelin significantly ($p < 0.05$) reduced pain in both the acetic acid-induced abdominal constriction response as well as the formalin-induced paw-licking reaction. In the report, the compound significantly improved pyrexia in rats in a dose-dependent manner. Pyrexia and analgesia are two typical symptoms of malaria infection. For most patients, absence of pyrexia, during malaria treatment is indicative of therapeutic success.

Protein-Ligand docking profiles of the compounds and pfLDH

To understand the possible mechanism by which the isolated compounds (friedelin, friedelinol, lupeol, and sitosterol) act, an in silico theoretical molecular docking approach was adopted using chloroquine, a known antimalarial drug, as a reference. The results revealed varying degrees of binding affinity and interaction patterns among the compounds (Fig. 5). Friedelinol and lupeol exhibited higher binding affinities (−8.455 kcal/mol and −8.277 kcal/mol, respectively) compared to Chloroquine (−7.442 kcal/mol) (Table S1), suggesting potentially stronger interactions with *pf*LDH. Furthermore, friedelinol formed the highest number of hydrogen bonds (4 bonds), while Chloroquine formed 3 hydrogen bonds, indicating their propensity for forming stable complexes with the target protein. The full fitness scores further supported the favourable binding modes of friedelinol and lupeol, with more negative values compared to Chloroquine, indicating their superior fitness in the binding pocket. Interestingly, the length of the compounds' interactions, ranging from 1.763 Å for friedelin to 2.64 Å for lupeol (Table S1), also influenced their effects, with longer interactions potentially leading to more stable binding. These findings suggest that friedelinol and lupeol possess promising antimalarial properties and merit further investigation as potential drug candidates targeting *pf*LDH. These reports corroborate the antiplasmodial activity reported in this research. In view of the structural similarity of friedelin and friedelinol, it could be hypothesized that the 3-hydroxy moiety of the steroidal framework could have accounted for the superior interactions with *pf*LDH than the carbonyl group at position three of the same framework. Friedelinol was tested as a mixture with friedelin, and its biological activity is not widespread compared to the latter. Based on these results, it is imperative to isolate and explore it potential for the management of malaria.

To better understand the variances in binding energies observed among the compounds, we utilized Pymol software and PBDSUM

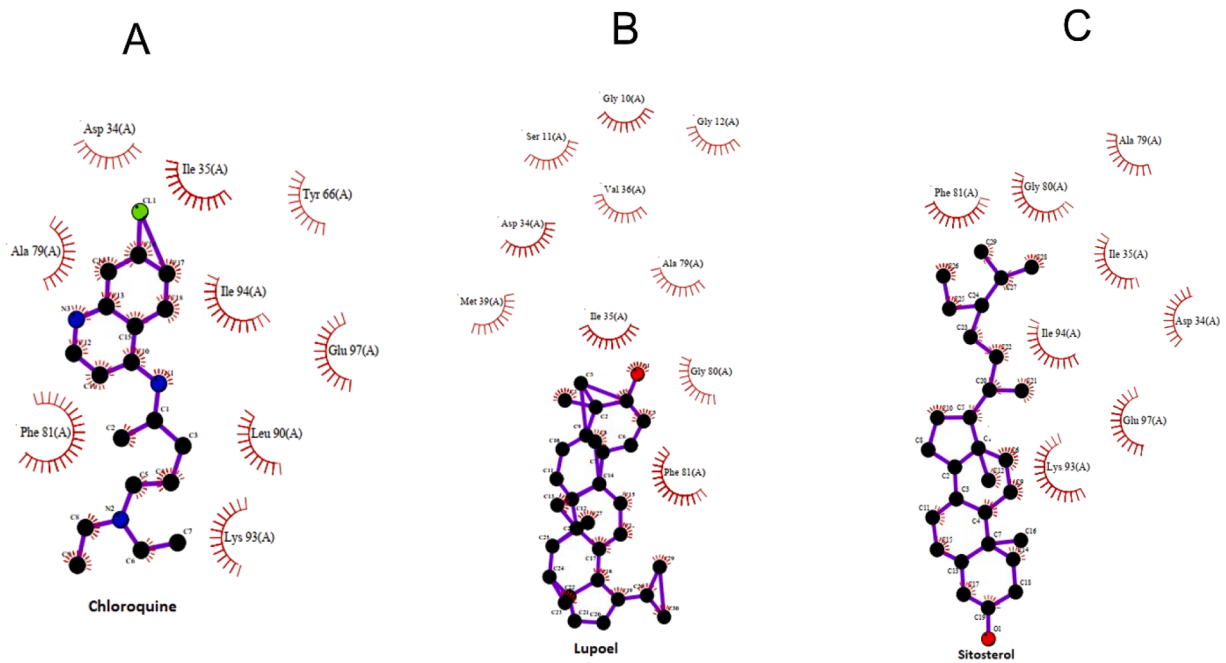

Fig. 6. Interactions established after docking of Chloroquine, Lupoel and Sitosterol with *pf*LDH. 2D plot showing both hydrogen and hydrophobic interactions in (A) Chloroquine/ *pf*LDH, (B) Complex Lupoel/ *pf*LDH and (C) Sitosterol/ *pf*LDH. The interacting residues are shown in the shaded arc with the respective number. The residues and the ligand are visualized as structure diagrams.

to analyse the docked complexes. Fig. 6 illustrates the interactions between the compounds and the target protein, highlighting the number and specific amino acid residues involved [28,58,59]. While the data for friedelin and friedelinol lacked a comprehensive interactive plot due to the 2D nature of these compounds, chloroquine, lupeol, and β-sitosterol exhibited common interactions with key residues such as Phe 81, Ile 35, and Ala 79 of *pf*LADH. Notably, chloroquine and β-sitosterol additionally interacted with Lys 93, Glu 97, and Ile 94 residues. Particularly, lupeol demonstrated a rich interaction profile, engaging with five specific residues including Met 39, Ser 11, Gly 10, Gly 11, and Val 36. Both lupeol and β-sitosterol were found to interact with Gly 80 and Asp 34 residues, akin to Chloroquine's binding pattern. These interactions suggest a combination of hydrophobic and hydrogen bonding interactions between the compounds and the amino acid residues of *pf*LDH, which could influence their overall binding affinities and potentially contribute to their antimalarial properties.

Pharmacokinetic and toxicity profile of the compounds

Analysis of the Adsorption, Distribution, Metabolism, Excretion (ADME) and toxicity profiles revealed intriguing characteristics of the compounds under investigation (Table S2 to S4). Chloroquine exhibited high lipophilicity (logP 4.733) and moderate water solubility (2.83×10^{-5} logmol/L), indicative of its potential for efficient absorption and distribution in biological systems (Table S2 and S3). Moreover, Chloroquine demonstrated high permeability across both MDCK and Caco2 cell monolayers, suggesting favourable intestinal absorption. These findings align with its known pharmacokinetic profile as an orally administered antimalarial agent [60, 61]. Additionally, Chloroquine showed high bioavailability (≈0.55) and blood-brain barrier (BBB) permeability (log BB 0.961) (Table S4). This is suggestive of its ability to penetrate the BBB, which is crucial for treating cerebral malaria. In contrast, β-sitosterol, friedelin, lupeol, and friedelinol exhibited varying ADME properties that may influence their pharmacokinetic behaviour. Sitosterol displayed extremely low water solubility (1.26×10^{-8} logmol/L) and moderate to low permeability across MDCK and Caco2 cell monolayers, indicating limited absorption potential (Table S2). However, its high logP value (8.106) suggests significant lipophilicity, which may contribute to its tissue distribution and bioactivity. Friedelin, lupeol, and friedelinol exhibited low water solubility and permeability, with logP values ranging from 6.656 to 7.216. These high logP values indicate that the compounds are highly lipophilic, which suggests they share similar pharmacokinetic properties, such as absorption, distribution, and tissue penetration and might have favourable membrane permeability but could face issues with solubility and distribution in aqueous environments.

The compounds exhibited diverse interactions with metabolic enzymes and drug transporters (Table 6). Chloroquine, for instance, displayed notable interactions with cytochrome P450 enzymes, particularly CYP2D6 and CYP3A4, indicating its potential as both a substrate and inhibitor of these enzymes. Sitosterol, friedelin, lupeol, and friedelinol also showed interactions with various cytochrome P450 enzymes, suggesting potential involvement in drug metabolism pathways. Additionally, the compounds demonstrated varying levels of susceptibility to P-glycoprotein-mediated efflux. Chloroquine and sitosterol were identified as substrates of this transporter, meaning that they are prone to being actively pumped out of cells by P-glycoprotein. This can significantly impact their bioavailability, as high efflux activity might reduce intracellular drug concentrations, potentially leading to reduced efficacy. It could also contribute to drug resistance, as the active efflux could lead to decreased drug retention within target cells. On the other hand, friedelin, lupeol, and friedelinol exhibited minimal interactions with P-glycoprotein, suggesting that they are less likely to be expelled from cells via this transporter. This characteristic could imply better bioavailability, as these compounds would be more likely to remain within cells and exert their therapeutic effects. This reduced interaction with P-glycoprotein might also indicate a lower risk of drug resistance due to efflux mechanisms, which is a significant concern in treating diseases like malaria.

The compounds with minimal P-glycoprotein interaction, like friedelin, lupeol, and friedelinol, could offer advantages in developing drugs with higher efficacy and lower resistance risk. This information is crucial for guiding drug formulation and optimizing therapeutic outcomes, especially in conditions where P-glycoprotein-mediated efflux plays a role in treatment resistance.

In terms of toxicity, evaluation of hERG inhibition, Ame's mutagenicity, and other toxicity endpoints (Table 7) indicated potential safety concerns for some compounds. Chloroquine exhibited moderate to high hERG inhibition (0.958) and genotoxicity (0.845), which are associated with cardiac arrhythmias and DNA damage, respectively [62]. Sitosterol, friedelin, lupeol, and friedelinol displayed lower hERG inhibition and genotoxicity scores, suggesting a potentially safer profile in these aspects [62,63].

Conclusion

Hydroethanol extract (70 %) of the stem of *Senegalia ataxacantha* shows anti-plasmodial and antipyretic activity *in vivo* and thus gives credence to its use in traditional medicine. Pentacyclic triterpenoids friedelin, friedelinol are reported for the first in the plant in addition to sitosterol and lupeol which are known constituents. These compounds showed *in vitro* anti-plasmodial activities and were predicted to inhibit parasite lactate dehydrogenase (pfLDH**).** Moderate interactions with cytochrome p450 enzymes based on *in silico* assessment was a concern but so far, the evidence generated points to a safe use of the plant.

Funding sources

This research did not receive any specific grant from funding agencies in the public, commercial, or not-for-profit sectors.

Ethics declaration

Animal experimental techniques were conducted after the study received ethical permission from the Committee on Animal Ethics

Table 6
Metabolic profile of the compounds.

	Substrates						Inhibitors						
Compound	CYP1A2	CYP2C19	CYP2C9	CYP2D6	CYP3A4	CYP2B6	CYP1A2	CYP2C19	CYP2C9	CYP2D6	CYP3A4	CYP2B6	CYP2C8
Chloroquine	0.09	0.73	0.00	0.37	1.00	0	0	0	0	0.006	0	0.999	0.003
Sitosterol	0.02	0.10	0.72	0.76	1.00	1	0	0	0.441	0.001	0	1	1
Friedelin	0.41	1.00	0.56	0.94	0.46	1	0	0.074	0.983	0.007	0	0.989	0.907
Lupeol	0.82	1.00	0.98	1.00	0.01	1	0	0.06	0.898	0	0	0.678	0.993
Friedalinol	0.20	1.00	0.22	0.90	0.39	1	0	0.002	0.968	0.003	0	0.578	0.759

Table 7
Toxicity profile of the compounds.

Compound	hERG	Ames	Skin Sensitive	Carcinogenicity	Respiratory	Neurotoxicity	Ototoxicity	Hematotoxicity	Nephrotoxicity	Genotoxicity	LD_{50} (mg kg^{-1})
Chloroquine	0.958	0.512	0.989	0.204	0.996	0.986	0.638	0.68	0.982	0.845	750
Sitosterol	0.397	0.037	0.16	0.353	0.75	0.272	0.882	0.137	0.127	0	1190
Friedelin	0.159	0.113	0.165	0.542	0.701	0.506	0.765	0.272	0.085	0.001	940
Lupeol	0.225	0.035	0.047	0.558	0.824	0.417	0.876	0.071	0.02	0	2000
Friedalinol	0.24	0.093	0.11	0.498	0.704	0.197	0.813	0.17	0.066	0	890

and Research, Department of Pharmacology, Kwame Nkrumah University of Science and Technology (KNUST/Cology 7/034). Furthermore, guidelines for the Helsinki Declaration for the care of experimental animals were meticulously observed.

Data availability

All datasets used and/or analysed during the current study are available in the manuscript as supplementary material and could also be assessed from corresponding author on reasonable request.

CRediT authorship contribution statement

Kennedy Ameyaw Baah: Conceptualization, Methodology, Formal analysis, Investigation, Resources, Data curation, Writing – original draft. **Akwasi Acheampong:** Conceptualization, Methodology, Resources, Writing – review & editing, Supervision, Project administration. **Isaac Kingsley Amponsah:** Conceptualization, Methodology, Formal analysis, Investigation, Resources, Data curation, Writing – original draft, Writing – review & editing, Supervision, Project administration. **Silas Adjei:** Methodology, Formal analysis, Writing – review & editing. **Yakubu Jibira:** Methodology, Formal analysis, Investigation, Resources, Writing – original draft, Writing – review & editing, Supervision. **Reinhard Isaac Nketia:** Methodology, Formal analysis, Investigation, Data curation, Writing – original draft. **Linda Mensah Sarpong:** Investigation, Data curation. **Emmanuel Quaye Kontoh:** Formal analysis, Data curation, Writing – review & editing.

Declaration of competing interest

The authors declare that they have no known competing financial interests or personal relationships that could have appeared to influence the work reported in this paper.

Supplementary materials

Supplementary material associated with this article can be found, in the online version, at doi:10.1016/j.sciaf.2024.e02455.

References

[1] WHO, World malaria World malaria report report. https://www.wipo.int/amc/en/mediation/%0Ahttps://www.who.int/teams/global-malaria-programme/reports/world-malaria-report-2023, 2023 (accessed: Jan. 31, 2024).
[2] WHO, World malaria report. https://www.who.int/teams/global-malaria-programme/reports/world-malaria-report-2022, 2022 (accessed: Jan. 31, 2024).
[3] W. Leal Filho, J. May, M. May, G.J. Nagy, Climate change and malaria: some recent trends of malaria incidence rates and average annual temperature in selected sub-Saharan African countries from 2000 to 2018, Malar. J. 22 (1) (2023) 248.
[4] A.B. Orok, O. Ajibaye, O.O. Aina, G. Iboma, S. Adagyo Oboshi, B. Iwalokun, Malaria interventions and control programes in Sub-Saharan Africa: a narrative review, Cogent. Med. 8 (1) (2021) 1940639.
[5] WHO, World malaria report. https://www.who.int/teams/global-malaria-programme/reports/world-malaria-report-2021, 2021 (accessed: Jan. 31, 2024).
[6] WHO, World malaria report. https://www.who.int/teams/global-malaria-programme/reports/world-malaria-report-2020, 2020 (accessed: Jan. 31, 2024).
[7] H.J. Oladipo, Y.A. Tajudeen, I.O. Oladunjoye, S.I. Yusuff, R.O. Yusuf, E.M. Oluwaseyi, M.O. AbdulBasit, Y.A. Adebisi, M.S. El-Sherbini, Increasing challenges of malaria control in sub-Saharan Africa: priorities for public health research and policymakers, Ann. med. surg. 81 (2022) 104366.
[8] S.K. Pandey, U. Anand, W.A. Siddiqui, R. Tripathi, Drug development strategies for malaria: with the hope for new antimalarial drug discovery—an update, Adv. Med. 2023 (2023) 1–10, https://doi.org/10.1155/2023/5060665.
[9] A.R. Parhizgar, A. Tahghighi, Introducing new antimalarial analogues of chloroquine and amodiaquine: a narrative review, Iran. J. Med. Sci. 42 (2) (2017) 115.
[10] K.A. Baah, A. Acheampong, I.K. Amponsah, R.I. Nketia, Antiplasmodial activity and phytochemical evaluation of the stems of *Albizia coriaria* and *Ficus sur*, European J. Med. Plants 35 (2) (2024) 1–10.
[11] L. Cui, S. Lindner, J. Miao, Translational regulation during stage transitions in malaria parasites, Ann. N. Y. Acad. Sci. 1342 (1) (2015) 1–9.
[12] N.N.D. Nortey, S. Korsah, M. Tagoe, J.A. Apenteng, F.A. Owusu, J. Oppong, A.E. Attah, S. Allotey, Herbs used in antimalarial medicines: a study in the greater accra region of ghana, evidence-based complement, Altern. Med. 2023 (2023).
[13] K. Cimanga, T. De Bruyne, L. Pieters, A.J. Vlietinck, C.A. Turger, In Vitro and in Vivo Antiplasmodial Activity of Cryptolepine and Related Alkaloids from *Cryptolepis sanguinolenta*, J. Nat. Prod. 60 (7) (1997) 688–691, https://doi.org/10.1021/NP9605246.
[14] G. Chianese, S.R. Yerbanga, L. Lucantoni, A. Habluetzel, N. Basilico, D. Taramelli, E. Fattorusso, O. Taglialatela-Scafati, Antiplasmodial triterpenoids from the fruits of neem, *Azadirachta indica*, J. Nat. Prod. 73 (8) (2010) 1448–1452.
[15] A. Maroyi, Review of Ethnopharmacology and phytochemistry of *Acacia ataxacantha*, Trop. J. Pharm. Res. 17 (11) (2018) 2301–2308.
[16] A.M.O. Amoussa, L. Lagnika, A. Sanni, *Acacia ataxacantha* (bark): chemical composition and antibacterial activity of the extracts, Int J Pharm Pharm Sci 6 (11) (2014) 138–141.
[17] A.M.O. Amoussa, L. Lagnika, M. Bourjot, C. Vonthron-Senecheau, A. Sanni, Triterpenoids from Acacia ataxacantha DC: antimicrobial and antioxidant activities, BMC Complement. Altern. Med. 16 (1) (Aug. 2016) 1–8, https://doi.org/10.1186/S12906-016-1266-Y/TABLES/4.
[18] Y. Touitou, F. Portaluppi, M.H. Smolensky, L. Rensing, Ethical Principles and Standards for the Conduct of Human and Animal Biological Rhythm Research, Chronobiol. Int. 21 (1) (2004) 161–170, https://doi.org/10.1081/CBI-120030045.
[19] OECD, Acute Oral Toxicity – Up-and-Down-Procedure (UDP), Oecd Guidel, Test. Chem. (2008).
[20] M.K. Baah, A.Y. Mensah, E. Asante-Kwatia, I.K. Amponsah, A.D. Forkuo, B.K. Harley, S. Adjei, In Vivo Antiplasmodial Activity of Different Solvent Extracts of *Myrianthus libericus* Stem Bark and Its Constituents in *Plasmodium berghei* -Infected Mice, Evidence-based Complement, Altern. Med. 2020 (2020), https://doi.org/10.1155/2020/8703197.
[21] W. Peters, J.H. Portus, B.L. Robinson, The chemotherapy of rodent malaria, XXII: the value of drug-resistant strains of *P. berghei* in screening for blood schizontocidal activity, Ann. Trop. Med. Parasitol. 69 (2) (1975) 155–171, https://doi.org/10.1080/00034983.1975.11686997.

[22] A. Nardos, E. Makonnen, *In vivo* antiplasmodial activity and toxicological assessment of hydroethanolic crude extract of *Ajuga remota*, Malar. J. 16 (1) (2017) 1–8, https://doi.org/10.1186/s12936-017-1677-3.

[23] S. Tesema, E. Makonnen, In Vivo Analgesic and Antipyretic Activities of N-Butanol and Water Fractions of *Ocimum Suave* Aqueous Leaves Extract in Mice, Ethiop. J. Health Sci. 25 (2) (Apr. 2015) 139, https://doi.org/10.4314/EJHS.V25I2.6.

[24] J. Kamau, M. Piero Ngugi, Antipyretic, Antiinflammatory and Antinociceptive Activities of Aqueous Bark Extract of *Acacia nilotica* (L.) Delile in Albino Mice, Pain Manag. Med 2 (2) (2016) 113, https://doi.org/10.35248/2684-1320.16.2.113.

[25] T. Yimer, Y.K. Emiru, Z.D. Kifle, A. Ewunetei, M. Adugna, E.M. Birru, Pharmacological Evaluation of Antipyretic and Antioxidant Activities of 80% Methanol Root Extract and Derived Solvent Fraction of *Echinops kebericho* M. (Asteraceae) in Mice Model, Biomed Res. Int. 2021 (2021), https://doi.org/10.1155/2021/6670984.

[26] M. Smilkstein, N. Sriwilaijaroen, J.X. Kelly, P. Wilairat, M. Riscoe, Simple and inexpensive fluorescence-based technique for high-throughput antimalarial drug screening, Antimicrob. Agents Chemother. 48 (5) (2004) 1803–1806.

[27] D.S. Wishart, C. Knox, A.C. Guo, S. Shrivastava, M. Hassanali, P. Stothard, Z. Chang, J. Woolsey, DrugBank: a comprehensive resource for in silico drug discovery and exploration, Nucleic. Acids. Res. 34 (suppl_1) (2006) D668–D672.

[28] F.C. Bernstein, T.F. Koetzle, G.J.B. Williams, E.F. Meyer Jr., M.D. Brice, J.R. Rodgers, O. Kennard, T. Shimanouchi, M. Tasumi, The Protein Data Bank: a computer-based archival file for macromolecular structures, Arch. Biochem. Biophys. 185 (2) (1978) 584–591.

[29] R.A. Laskowski, J. Jabłońska, L. Pravda, R.S. Vařeková, J.M. Thornton, PDBsum: structural summaries of PDB entries, Protein Sci. 27 (1) (2018) 129–134.

[30] A. Grosdidier, V. Zoete, O. Michielin, SwissDock, a protein-small molecule docking web service based on EADock DSS, Nucleic. Acids. Res. 39 (suppl_2) (2011) W270–W277.

[31] M.F. Adasme, K.L. Linnemann, S.N. Bolz, F. Kaiser, S. Salentin, V.J. Haupt, M. Schroeder, PLIP 2021: expanding the scope of the protein–ligand interaction profiler to DNA and RNA, Nucleic. Acids. Res. 49 (W1) (2021) W530–W534.

[32] A. Daina, O. Michielin, V. Zoete, SwissADME: a free web tool to evaluate pharmacokinetics, drug-likeness and medicinal chemistry friendliness of small molecules, Sci. Rep. 7 (1) (2017) 42717.

[33] M.N. Drwal, P. Banerjee, M. Dunkel, M.R. Wettig, R. Preissner, ProTox: a web server for the in silico prediction of rodent oral toxicity, Nucleic. Acids. Res. 42 (W1) (2014) W53–W58.

[34] N.S.S. Ambarwati, B. Elya, A. Malik, M. Hanafi, H. Omar, Isolation, characterization, and antibacterial assay of friedelin from *Garcinia latissima* Miq. leaves, J. Phys.: Conference Series (2019) 55078. IOP Publishing.

[35] K. Day, A. Tripathi, Arrangement graphs: a class of generalized star graphs, Inf. Process. Lett. 42 (5) (1992) 235–241, https://doi.org/10.1016/0020-0190(92)90030-Y.

[36] S.B. Mahato, A.P. Kundu, Review Article Number 98 13C Nmr Spectra of Pentacyclic Triterpenoids-a and Some Salient Features, Science (1979) 37 (6) (1994) 1517–1575 (80-.).

[37] G.C.M. Salazar, G.D.F. Silva, L.P. Duarte, S.A. Vieira Filho, I.S. Lula, Two epimeric friedelane triterpenes isolated from *Maytenus truncata* Reiss: 1H and 13C chemical shift assignments, Magn. Reson. Chem. 38 (11) (2000) 977–980.

[38] S.N. Mathias, K. Abubakar, N. October, M.S. Abubakar, H.E. Mshelia, Anti-venom potentials of friedelin isolated from hexane extract fraction of *Albizia chevalieri* hams (Mimosaceae), Ife J. Sci. 18 (2) (2016) 473–482.

[39] M.H. Radi, R.A. El-Shiekh, A.M. El-Halawany, E. Abdel-Sattar, Friedelin and 3β-Friedelinol: pharmacological Activities, Rev. Bras. Farmacogn. 33 (5) (Jun. 2023) 886–900, https://doi.org/10.1007/S43450-023-00415-5, 2023 335.

[40] M.M. Ododo, M.K. Choudhury, A.H. Dekebo, Structure elucidation of β-sitosterol with antibacterial activity from the root bark of *Malva parviflora*, Springerplus. 5 (2016) 1–11.

[41] M.O. Aliba, I.G. Ndukwe, H. Ibrahim, Isolation and characterization of B-sitosterol from methanol extracts of the stem bark of large-leaved rock fig (*Ficus abutilifolia* Miq), J. Appl. Sci. Environ. Manag. 22 (10) (2018) 1639–1642.

[42] S. Gurupriya, L. Cathrine, P. Pratheema, HPTLC method for the determination of lupeol from *Andrographis echioides* leaves, Int J Pharm Pharm Sci 10 (2018) 102–107.

[43] A.P. Dantanarayana, N.S. Kumar, M.U.S. Sultanbawa, S. Balasubramaniam, Structures of four new oxygenated lupanes from *Pleurostylia opposita* (Celastraceae), J. Chem. Soc. Perkin Trans. 1 (1981) 2717–2723.

[44] M.M. Mailafiya, U.U. Pateh, H.S. Hassan, M.I. Sule, A.H. Bila, T.L. Musa, V. Atinga, J.I. AchikaM, Isolation of lupeol from the stem bark of *Leptadenia hastata* (Pers.) Decne, J. Appl. Sci. Environ. Manag. 24 (10) (2020) 1835–1838.

[45] A.M.O. Amoussa, L. Lagnika, M. Tchatchedre, A. Laleye, A. Sanni, Acute toxicity and antifungal effects of *Acacia ataxacantha* (Bark), Int. J. Pharmacogn. Phytochem. Res. 7 (4) (2015) 661–668.

[46] T.C. Akapa, S.M. Obidola, F.O. Philip, Loperamide induced constipated Wister rats: laxative role of aqueous extract of *Acacia ataxacantha* leaves, World J Pharm Pharma Sci 3 (12) (2014) 189–199.

[47] B. Chipwaza, J.P. Mugasa, I. Mayumana, M. Amuri, C. Makungu, P.S. Gwakisa, Self-medication with anti-malarials is a common practice in rural communities of Kilosa district in Tanzania despite the reported decline of malaria, Malar. J. 13 (2014) 1–11.

[48] D.A. Fidock, P.J. Rosenthal, S.L. Croft, R. Brun, S. Nwaka, Antimalarial drug discovery: efficacy models for compound screening, Nat. Rev. Drug Discov. 3 (6) (2004) 509–520.

[49] P.J. Waako, B. Gumede, P. Smith, P.I. Folb, The *in vitro* and *in vivo* antimalarial activity of *Cardiospermum halicacabum* L. and *Momordica foetida* Schumch. Et Thonn, J. Ethnopharmacol. (2005), https://doi.org/10.1016/j.jep.2005.02.017.

[50] V. Muñoz, M. Sauvain, G. Bourdy, J. Callapa, S. Bergeron, I. Rojas, J.A. Bravo, L. Balderrama, B. Ortiz, A. Gimenez, E. Deharo, A search for natural bioactive compounds in Bolivia through a multidisciplinary approach. Part I. Evaluation of the antimalarial activity of plants used by the Chacobo Indians, J. Ethnopharmacol. (2000), https://doi.org/10.1016/S0378-8741(99)00148-8.

[51] B. Emsen, T. Engin, H. Turkez, Vitro investigation of the anticancer activity of friedelin in glioblastoma multiforme glioblastoma Multiformede Friedelinin Antikanser Aktivitesinin in vitro Incelenmesi, AKU J. Sci. Eng 18 (2018) 763–773, https://doi.org/10.5578/fmbd.67733.

[52] A.G.B. Azebaze, A.B. Dongmo, M. Meyer, B.M.W. Ouahouo, A. Valentin, E.Laure Nguemfo, A.E. Nkengfack, W. Vierling, Antimalarial and vasorelaxant constituents of the leaves of *Allanblackia monticola* (Guttiferae), Ann. Trop. Med. Parasitol. 101 (1) (Jan. 2007) 23–30, https://doi.org/10.1179/136485907x157022.

[53] A. Singh, H.M. Mukhtar, H. Kaur, L. Kaur, Investigation of antiplasmodial efficacy of lupeol and ursolic acid isolated from *Ficus benjamina* leaves extract, Nat. Prod. Res. 34 (17) (Sep. 2020) 2514–2517, https://doi.org/10.1080/14786419.2018.1540476.

[54] P. Chaniad, A. Chukaew, A. Payaka, A. Phuwajaroanpong, T. Techarang, W. Plirat, C. Punsawad, Antimalarial potential of compounds isolated from *Mammea siamensis* T. Anders. flowers: *in vitro* and molecular docking studies, BMC Complement. Med. Ther. 22 (1) (Dec. 2022), https://doi.org/10.1186/S12906-022-03742-7.

[55] J.K. Mworia, C.M. Kibiti, M.P. Ngugi, J.N. Ngeranwa, Antipyretic potential of dichloromethane leaf extract of *Eucalyptus globulus* (Labill) and *Senna didymobotrya* (Fresenius) in rats models, Heliyon. 5 (12) (Dec. 2019) e02924, https://doi.org/10.1016/J.HELIYON.2019.E02924.

[56] M.Y. Abbas, J.I. Ejiofor, A.H. Yaro, M.I. Yakubu, J.A. Anuka, Anti inflammatory and antipyretic activities of the methanol leaf extract of *Acacia ataxacantha* D.C. (Leguminosae) in mice and rats, Bayero J. Pure Appl. Sci. 10 (1) (Sep. 2017) 1–5, https://doi.org/10.4314/BAJOPAS.V10I1.1.

[57] P. Antonisamy, V. Duraipandiyan, S. Ignacimuthu, Anti-inflammatory, analgesic and antipyretic effects of friedelin isolated from *Azima tetracantha* Lam. in mouse and rat models, J. Pharm. Pharmacol. 63 (8) (Jun. 2011) 1070–1077, https://doi.org/10.1111/J.2042-7158.2011.01300.X.

[58] M. Fricker, M.J. Oliva-Martín, G.C. Brown, Primary phagocytosis of viable neurons by microglia activated with LPS or Aβ is dependent on calreticulin/LRP phagocytic signalling, J. Neuroinflammation 9 (2012) 1–12.

[59] D.B. Kitchen, H. Decornez, J.R. Furr, J. Bajorath, Docking and scoring in virtual screening for drug discovery: methods and applications, Nat. Rev. Drug Discov. 3 (11) (2004) 935–949.

[60] M. Delves, D. Plouffe, C. Scheurer, S. Meister, S. Wittlin, E.A. Winzeler, R.E. Sinden, D. Leroy, The activities of current antimalarial drugs on the life cycle stages of Plasmodium: a comparative study with human and rodent parasites, PLoS. Med. 9 (2) (2012) e1001169.
[61] J. Ducharme, R. Farinotti, Clinical pharmacokinetics and metabolism of chloroquine: focus on recent advancements, Clin. Pharmacokinet. 31 (1996) 257–274.
[62] A. Garrido, A. Lepailleur, S.M. Mignani, P. Dallemagne, C. Rochais, hERG toxicity assessment: useful guidelines for drug design, Eur. J. Med. Chem. 195 (2020) 112290.
[63] D.J. Leishman, M.M. Abernathy, E.B. Wang, Revisiting the hERG safety margin after 20 years of routine hERG screening, J. Pharmacol. Toxicol. Methods 105 (2020) 106900.